Synthesis of Augmented Biofuel Processes Using Solar Energy

Dharik S. Mallapragada
School of Chemical Engineering, Purdue University, West Lafayette, IN 47907

Mohit Tawarmalani
Krannert School of Management, Purdue University, West Lafayette, IN 47907

Rakesh Agrawal
School of Chemical Engineering, Purdue University, West Lafayette, IN 47907

DOI 10.1002/aic.14456
Published online April 11, 2014 in Wiley Online Library (wileyonlinelibrary.com)

A method for synthesizing augmented biofuel processes, which improve biomass carbon conversion to liquid fuel (η_{carbon}) using supplemental solar energy as heat, H_2, and electricity is presented. For a target η_{carbon}, our method identifies augmented processes requiring the least solar energy input. A nonconvex mixed integer nonlinear programming model allowing for simultaneous mass, heat, and power integration, is built over a process superstructure and solved using global optimization tools. As a case study, biomass thermochemical conversion via gasification/Fischer–Tropsch synthesis and fast-hydropyrolysis/hydrodeoxygenation (HDO) is considered. The optimal process configurations can be categorized either as standalone ($\eta_{carbon} \leq 54\%$), augmented using solar heat ($54\% \leq \eta_{carbon} \leq 74\%$), or augmented using solar heat and H_2 ($74 \leq \eta_{carbon} \leq 95\%$). Importantly, the process H_2 consumption is found to be close to the derived theoretical minimum values. To accommodate for the intermittency of solar heat/H_2, we suggest processes that can operate at low and high η_{carbon}. © 2014 American Institute of Chemical Engineers *AIChE J*, 60: 2533–2545, 2014
Keywords: process synthesis, optimization, energy, mathematical modeling

Introduction

The widespread use of renewable energy sources like solar energy in lieu of fossil fuels has the potential to reduce global CO_2 emissions. However, when compared to fossil fuels, renewable energy sources have relatively low energy intensity and are intermittently available. This introduces new challenges in meeting various energy demands.[1,2] Among them is the challenge of producing high energy density fuels that can be utilized for transportation and are also compatible with the existing liquid fuel infrastructure. The continued use of liquid hydrocarbons for transportation relies on the availability of renewable carbon sources. The biomass gathered as waste from existing agriculture and forestry practices and grown on agriculturally degraded land with minimal energy input, constitutes the sustainably available (SA) biomass carbon resource.[3–6] The quantity of liquid fuel or biofuel produced from SA biomass is dependent on the process carbon recovery (η_{carbon}), defined as the fraction of total biomass carbon recovered in the biofuel. Existing thermochemical and biochemical standalone processes, which use biomass as the main energy source, are reported to produce between 6.7 and 10.9 MJ of biofuel/kg of biomass.[3,6–8] For typical carbon contents in biomass and biofuel, which are approximately 50 and 85 wt %, respectively, and assuming a biofuel energy content of 42 MJ/kg, this translates to $\eta_{carbon} = 27$–44% for such standalone processes. This low range of η_{carbon} has the following implications. First, using all of the US SA biomass resource, estimated to be between 500 and 1000 million metric tons per year (MMT/y),[6,9] standalone biofuel processes can only supply ~22–44% of the current US transportation fuel demand.[3,10] Second, these processes diminish the impact of using biomass toward reducing global CO_2 emissions, as they release >50% of the captured atmospheric carbon as CO_2. Third, the relatively low biofuel yield (or η_{carbon}) of standalone processes is a contributing factor to their unfavorable economics.[11] Not surprisingly, despite several process optimization efforts and government policy incentives, globally, few biofuel processes have been commercially successful.[12] To increase the carbon recovery and in turn the biofuel yield, the proposed use of supplemental energy forms during biofuel production[13,14] defines a new class of technologies termed as augmented biofuel processes.[3] The use of supplemental energy in the form of solar-derived H_2, heat, or electricity in lieu of biomass for process energy requirements, makes it theoretically possible to recover ~100% of the biomass carbon atoms as biofuel. In the US context, augmented processes with $\eta_{carbon} \sim 100\%$ can potentially supply ~100% of the current transportation fuel demand using 1000 MMT/y of SA biomass.[10,13]

Here, we present a framework for synthesizing augmented biofuel processes, starting from a set of biomass conversion pathways and supplemental energy inputs like solar heat, electricity, and H_2. We formulate a mixed integer nonlinear programming (MINLP) model that allows for simultaneous

Additional Supporting Information may be found in the online version of this article.

Correspondence concerning this article should be addressed to R. Agrawal at agrawalr@purdue.edu.

Correction added on April 22, 2014 after online publication: order of authors.

mass, heat, and power integration over a derived process superstructure. For every target value of η_{carbon}, the solution of the MINLP model, obtained using global optimization tools, identifies the biofuel process configuration requiring the least solar energy input as heat, electricity, and H_2. These supplementary energy inputs can be recovered at higher solar energy conversion efficiencies than harvesting additional biomass via photosynthesis.[3] In this manner, the chosen objective function also minimizes the land area requirement for biofuel production. Additionally, as solar energy system costs (e.g., capital cost) are significantly impacted by the system efficiency of harnessing solar energy,[15] the chosen objective function indirectly contributes toward improving the process economics. To address the intermittency of solar energy availability, we identify robust biofuel process designs that are capable of operating either in standalone (low η_{carbon}) or augmented (high η_{carbon}) process modes. If this flexibility in process carbon recovery can be attained without start-up and shutdown of units, then the process can be operated continuously even if cost-effective solar energy storage methods are not available. Alternatively, the identified augmented biofuel processes can operate round the clock by integrating with renewable energy storage systems.[16] In a transition scenario, coal and natural gas can supplement biomass during times of solar energy unavailability.[14,17–21]

Example Superstructure

We discuss the augmented process synthesis model by considering two example biomass thermochemical pathways: (1) heat-assisted gasification followed by Fischer–Tropsch (FT) synthesis and (2) fast-hydropyrolysis followed by catalytic hydrodeoxygenation (HDO). Heat-assisted gasification produces a synthesis gas (syngas) mixture rich in H_2 and CO from the reaction of biomass with steam at temperatures close to 1000 K. This endothermic reaction requires the use of an external heat source (solar heat in this study). The additional heat soaked up during solar thermal driven heat-assisted gasification (referred as STG) results in the syngas having ~30% higher energy content than the feed biomass.[22,23] In contrast, direct biomass gasification using air or enriched oxygen (along with steam) results in undesirable CO_2 formation from biomass combustion. Such a gasifier will produce syngas with lower energy content than the feed biomass and, therefore, has not been considered here. The syngas exiting the heat-assisted gasifier is subsequently converted to liquid fuel via a suitable catalytic process like FT synthesis. The carbon recovery of the STG-FT process, by virtue of the additional solar energy stored in the syngas, is estimated to be higher than standalone gasification-FT processes.[22–24] To further enhance the carbon recovery, the unconverted reactants and by-products from FT synthesis can be recycled to the STG unit along with supplementary H_2.[24]

Alternatively, biomass can be processed via fast-hydropyrolysis or the fast-pyrolysis of biomass in presence of H_2 and a catalyst at temperatures near 700–800 K.[14] The exhaust from fast-hydropyrolysis, after removal of the solid char and ash, are fed to a lower temperature HDO reactor followed by condensation to produce a high energy density liquid fuel and gas by-products.[14,25] Fast-hydropyrolysis/HDO has been proposed as an improvement to biomass fast-pyrolysis in an inert atmosphere which produces a low energy density liquid product (known as bio-oil). The bio-oil produced from fast-pyrolysis is unstable due to the 35–40 wt % oxygen present and needs further upgrading via hydrotreating under high H_2 pressures (100–200 bar) for producing a transportation fuel.[26] By avoiding intermediate bio-oil formation, fast-hydropyrolysis/HDO processes (referred as H_2Bioil) can potentially overcome the challenges of fast-pyrolysis/hydrotreating processes while achieving similarly high energy and carbon efficiencies.[14,25,27] Recent proof-of-concept tests in a semicontinuous process report the production of a liquid fuel in the diesel and gasoline range, along with gas-phase products including C_1—C_3 hydrocarbons, solid char, and ash.[25,28] The H_2Bioil process can be operated with H_2 sourced from either gasifying a portion of the biomass or using supplemental solar H_2.[27] Additionally, the by-product gas and char could be reformed to produce syngas which provides an indirect source of H_2.[25] In a transition scenario, use of H_2 derived from coal, natural gas, or nuclear energy for the H_2Bioil process offers an economically competitive liquid fuel option.[11,14]

To simultaneously consider the process alternatives discussed above, we construct a process superstructure shown in Figure 1, referred as H_2Bioil-STG. For simplicity, Figure 1 only shows the main units and their process connectivities, and does not depict the intermediate compressors, heaters/coolers, heat exchangers, splitters, mixers, and other auxiliary units included as part of the superstructure. The biomass feed is split between a purge stream to be combusted for process heat, the H_2Bioil process, and the heat-assisted gasifier. The vapor stream from the H_2Bioil process is cooled and condensed to separate water, gaseous by-products, and crude liquid fuel. The char and ash, recovered from the H_2Bioil process, are either purged or used as feeds to the heat-assisted gasifier. Syngas is produced from the heat-assisted gasifier using one or more of the following feeds: biomass, char, and gas by-products from H_2Bioil process, residual CO_2, recycle gas from FT synthesis, steam, and solar H_2. After solid separation using a cyclone, the high temperature syngas is split between the H_2Bioil process, syngas cleaning or purged to be combusted for process heat. As part of syngas cleaning, the Water-Gas Shift (WGS) reactor adjusts the syngas H_2/CO molar ratio to near 2, as needed for FT synthesis. The adjusted syngas is cooled to condense water and sent for acid gas removal. A Rectisol unit is used to remove 97% CO_2 and 100% sulfur (if present, as H_2S) from the syngas while requiring electrical power input for refrigeration and low pressure steam for solvent regeneration.[31] The clean syngas stream is compressed, heated, and fed to FT synthesis to produce a mixture of C_1—C_4 hydrocarbons, naphtha, diesel, and wax range alkanes. The FT exhaust is fed to the product upgrading unit, where a wax hydrocracker is used to increase the yield of diesel range alkanes. The exhaust stream from the hydrocracker is subsequently cooled and separated using a three-phase separator into crude liquid fuel, recycle gas, and water. The purge streams of the superstructure in Figure 1 are combusted using external air to recover a portion of their heating value for process heat. The superstructure in Figure 1 assumes that all the biomass fed is converted via either reaction or combustion. The main topological process variables of interest are: (1) the split fraction of input biomass to the two thermochemical pathways, (2) the extent of recycling of unconverted gases, solids, and residual CO_2 as well as (3) the fraction of syngas used to supply H_2 to the H_2Bioil process.

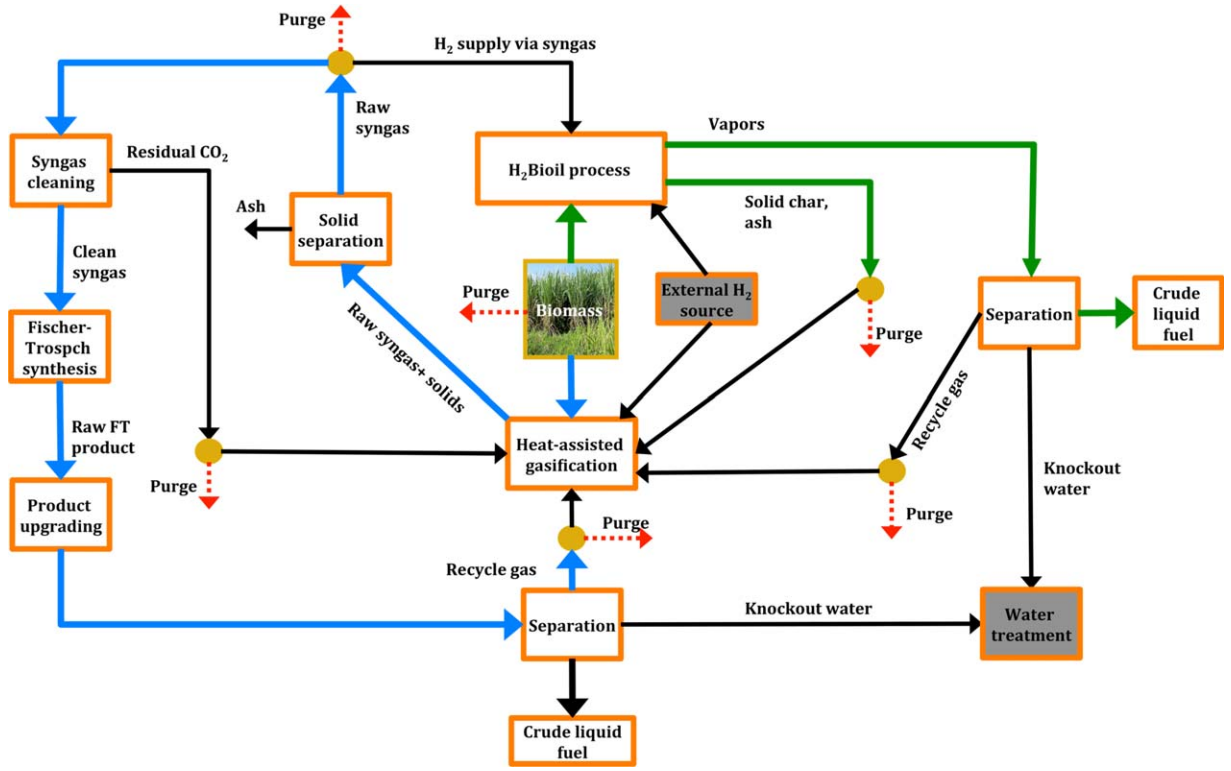

Figure 1. Simplified representation of H_2Bioil-STG superstructure.

Gasification-FT pathway marked in blue, fast-hydropyrolysis/HDO pathway marked in green. All the purge streams (dotted red) are utilized for their heating value via combustion. The shaded units have not been modeled here. [Color figure can be viewed in the online issue, which is available at wileyonlinelibrary.com.]

Mathematical Model

We develop an MINLP model describing the H_2Bioil-STG superstructure using the mass, energy balances, and other physical constraints governing each of the unit operations and the streams involved. The formulation size and nonconvexity are managed to enable the use of global optimization tools, without compromising on accuracy. Toward this end, we make certain justifiable simplifications in modeling units whose influence on the process output is small relative to that of the other modeled process units. Here, we summarize the key features of the MINLP model, with remaining aspects more elaborately explained in Supporting Information. All the notations used below is described after the conclusions section.

The major decision variables for the optimization include: (1) the individual component molar flows and total flows for each stream in the superstructure, (2) split fractions of stream splitters, (3) heating or cooling requirements for each unit, (4) flow rates and power output of Rankine cycles utilizing waste heat, and (5) other parametric variables (binary or continuous) associated with each unit. The temperatures of the individual streams are assumed to be the same as the temperature of the corresponding originating unit, which are assumed to be constant. To simplify the models for heat exchange and power generation, we have neglected the thermal energy available from cooling the multicomponent streams produced from FT synthesis/hydrocracking and the H_2Bioil process below their dew point temperatures. Instead, we only consider the thermal energy available from cooling these streams to 523 K (which is close to their typical dew points) for heat exchange with other process streams and/or power generation. A portion of the low temperature heat available from subcooling these multicomponent streams below 523 K can be used to dry the woody biomass from a typical as-received moisture content of 50%[32] to the desired amount (Table 1). Pressure drops across the streams and units of the process are neglected and the variation of enthalpy with pressure is ignored for all components except water (steam). All the relevant thermodynamic data have been derived from either the Aspen properties database (from Aspen Plus®[33]) or NIST Chemistry Web Book.[34]

H_2Bioil process

Because fast-hydropyrolysis/HDO as a thermochemical pathway has only recently received attention in the literature,[14,25] a complete product description is not yet available. Here, we improve on our previous modeling efforts[27] by developing a stoichiometric model for the fast-hydropyrolysis/HDO reaction, which is used to model the H_2Bioil process. The model, given by Eq. 1, considers the reactants

Table 1. Biomass Feedstock Assumptions

	Values
wt % feed moisture, r^{moist}	7
wt % Carbon (dry)	50.60
wt % Hydrogen (dry)	6.08
wt % Oxygen (dry)	40.75
wt % Nitrogen (dry)	0.64
wt % Ash (dry)	1.93
LHV, MJ/kg	18.21

Data adapted from Ref. 32.

Table 2. Composition of Liquid Fuel Produced from H_2Bioil Process

Compounds	Formula	Composition/wt %
2,5-Xylenol	$C_8H_{10}O$	11.7
n-Heptane	C_7H_{16}	2.4
1-Trans-3,5-trimethyl cyclohexane	C_9H_{18}	7.4
3,3,5 Trimethyl heptane	$C_{10}H_{22}$	3.0
n-Propyl cyclohexane	C_9H_{18}	7.4
1,2,3-Trimethylbenzene	C_9H_{12}	1.0
n-Butyl-cyclohexane	$C_{10}H_{20}$	0.4
1,2 Dimethyl-3-ethylbenzene	$C_{10}H_{14}$	2.4
Cis-decalin	$C_{10}H_{18}$	4.8
n-Tridecane	$C_{13}H_{28}$	13.1
1,2,4-Triethyl benzene	$C_{12}H_{18}$	4.8
Bicyclohexyl	$C_{12}H_{22}$	0.4
Diphenyl	$C_{12}H_{10}$	6.6
Diamantane	$C_{14}H_{20}$	13.1
Phenanthrene	$C_{14}H_{10}$	9.2
n-Pentadecylcyclopentane	$C_{20}H_{40}$	0.4
Chrysene	$C_{18}H_{12}$	9.3
p-Xylene	C_8H_{10}	2.6

Data adapted from Ref. 32.

of woody biomass and H_2, producing a high energy density liquid fuel, gas, water, and solids.[25] The liquid fuel is assumed to have the same composition as the fast pyrolysis-hydrotreating liquid product as shown in Table 2.[32] The gas by-products include CO_2, C_1—C_3 hydrocarbons, and inert N_2. The presence of CO is neglected with the knowledge that *in situ* WGS reaction is expected to be favorable during fast-hydropyrolysis/HDO due to the large excess of water present as deoxygenation product.[14] Furthermore, H_2 is assumed to be present as a limiting reactant. Equation 1 is specified by the stoichiometric coefficients z_1-z_9, where $z_1 = 1$ is the reference, and z_3 refers to the fraction of biomass carbon recovered in the liquid product ($\eta_{\text{carbon,hyp}}$).

Among the few experimental publications on fast-hydropyrolysis/HDO, Marker et al. reported product distribution data obtained from semicontinuous experiments that used woody biomass and where catalyst, temperature, space velocity, and H_2 partial pressure were varied in certain ranges.[25,28] Using the parameter estimation model of Eq. 2, we estimate the value of the coefficients of Eq. 1 that best fits the experimental product distribution reported by Marker et al.[25,28] The objective function in Eq. 2 minimizes the sum of the least square error between model prediction and experimental data ($w_{i,j}^{\text{exp}}$), subject to the atom balance across the process. For the eight experimental data sets available for woody biomass fast-hydropyrolysis/HDO (see Supporting Information Table S6), the optimal solution of the model of Eq. 2 corresponds to $z_3 = \eta_{\text{carbon,hyp}} = 46\%$. We divide the experimental datasets into two groups corresponding to low (four datasets) and high (four datasets) carbon recovery cases, which allow us to investigate the sensitivity of the MINLP model results to the value of $\eta_{\text{carbon,hyp}}$. The optimal solution when considering eight datasets ($\eta_{\text{carbon,hyp}} = 46\%$), the low carbon recovery datasets ($\eta_{\text{carbon,hyp}} = 43\%$), and the high carbon recovery datasets ($\eta_{\text{carbon,hyp}} = 48\%$) are reported in Table 3. Notice that the objective function value of the low and high carbon recovery cases are lower than the value for $\eta_{\text{carbon,hyp}} = 46\%$, indicating a better fit to the experimental data. In accordance with reaction temperatures reported for the experimental datasets,[25,28] the H_2Bioil process is assumed to operate at an average temperature of 673 K for the $\eta_{\text{carbon,hyp}} = 43\%$ and $\eta_{\text{carbon,hyp}} = 48\%$ cases. For the process energy balance, even though the fast-hydropyrolysis/HDO reaction is expected to be mildly exothermic,[14,25] the enthalpy change of reaction is conservatively assumed to be the same as biomass fast-pyrolysis[35]

$$z_1 C_1 H_{1.44} O_{0.60} + z_2 H_2 \rightarrow z_3(\text{liquid}) + z_4 CO_2 + z_5 CH_4 + z_6 C_2H_6 + z_7 C_3H_8 + z_8 H_2O + z_9 \text{Char} \quad (1)$$

$$\text{Minimize} \sum_{j=1}^{m_{\text{exp}}} \sum_{i=2}^{9} \left(b_i z_i - w_{i,j}^{\text{exp}} \right)^2$$

$$\text{Subject to} \quad (2)$$

$$\sum_{i=1}^{9} \beta_{i,k} z_i = 0 \;\; k = \text{C, H, O}$$

$$z_1 = 1$$

$$z_i \geq 0 \;\; \forall i = 1, \ldots, 9$$

Table 3. Main Parameters-Biomass Processing

Parameter	Symbol	Values
H_2Bioil Process		
Temperature	$T_{\text{hyp},udd}$	673 K
Pressure	$P_{\text{hyp},udd}$	35 atm
Carbon recovery in liquid	$z_3 = \eta_{\text{carbon,hyp}}$	0.435, 0.457, 0.480
Optimal objective in Eq. 2		0.011, 0.024, 0.007
H_2 coefficient in Eq. 1	z_2	0.41, 0.47, 0.52
CO_2	z_4	0.08, 0.08, 0.08
CH_4	z_5	0.07, 0.08, 0.09
C_2H_6	z_6	0.05, 0.05, 0.05
C_3H_8	z_7	0.02, 0.03, 0.03
H_2O	z_8	0.43, 0.44, 0.44
Char (C)	z_9	0.25, 0.21, 0.17
Enthalpy change	ΔH_{pyro}	1.5 MJ/kg biomass fed[35]
Heat-Assisted Gasifier		
Temperature	$T_{gfy,udd}$	1400 K
Pressure	$P_{gfy,udd}$	35 atm
Maximum steam feed	Steam^{UB}	4 kmol/h
WGS equilibrium constant	$K_{wgs,gfy}^{\text{eq}}$	0.45
Methanation equilibrium constant	$K_{\text{meth},gfy}^{\text{eq}}$	1.72×10^{-5}

All the flow rates are normalized to 1 kmol/h of biomass carbon feed processed. Multiple values (separated by commas) considered for certain parameters.

Heat-assisted gasification

The heat-assisted gasifier is modeled as an equilibrium reactor operating at a temperature of 1400 K and a pressure of 35 atm (Table 3). It produces syngas composed of H_2, CO, CO_2, H_2O, CH_4, and N_2. Such high gasification temperatures virtually eliminate tar formation,[22,37] reduce the presence of higher hydrocarbons (other than CH_4) to trace amounts,[37] and also ensure that the reactions approach the equilibrium conditions.[38–40] The syngas composition is dependent on the variable flow rates and the compositions of the input streams, specifically, steam, solar H_2, biomass feed, recycle gas, and char to the gasifier. The equilibrium syngas composition is calculated using the equilibrium conditions for the WGS and CO-methanation reactions as well as the overall C, H, O atom balance (see Supporting Information). In particular, by altering the steam flow rate, the energy content of the syngas can be changed and so can the percentage of solid char and biomass that is converted to gas. Steam is necessary for converting the carbon in the biomass to CO and H_2, and allows for storing solar heat as the enthalpy of the syngas components. However, when the amount of steam is increased, the H_2/CO ratio and the fraction of the biomass carbon atoms oxidizing to undesirable CO_2 are expected to increase.[41,42] At the same time, additional solar energy soaked up as sensible heat during the conversion of additional water to steam reduces the fraction of solar energy input stored as liquid fuel.

FT synthesis and upgrading

We assume that cobalt catalysts are used, which increase wax production that can subsequently be hydrocracked to produce diesel range linear alkanes.[43,44] In addition, the CO conversion per pass was chosen to be 90%, based on the knowledge that WGS reaction activity is not significant for cobalt catalysts.[45,46] The reader is referred to Supporting Information Figure S1 for a brief overview of the literature pertaining to FT reactors and the syngas conversions reported therein. In general, FT product distribution is well-represented by the Anderson–Schulz–Flory distribution, which is a function of the carbon chain growth probability parameter, α.[43] Higher α promotes carbon chain growth, leading to higher wax and lower light gas ($<C_{10}$) production. The produced wax can be selectively converted via hydrocracking to diesel range molecules. In this manner, FT catalysts corresponding to the highest $\alpha(\leq 1)$ can increase diesel production.[43] Commercial FT catalysts that correspond to α as high as 0.96 have been reported in the literature.[47] Representative compounds have been used to model the presence of each lumped product group: CH_4, C_2H_6, C_3H_8, C_4H_{10} (C_1—C_4), and C_6H_{14} (naphtha or C_5—C_9) for less than C_{10}; $C_{15}H_{32}$ (diesel) for C_{10}—C_{20}; and $C_{25}H_{52}$ (wax) for greater than $C_{20}+$. The base case results are calculated using the lumped product distribution corresponding to $\alpha = 0.95$, whereas $\alpha = 0.98$ and $\alpha = 0.90$ cases are considered for analyzing the sensitivity of the model results with respect to α.

Downstream from the FT synthesis, the mild hydrocracking of the paraffinic wax forms products with carbon yields that can be reasonably approximated as consisting of 80% diesel ($C_{15}H_{32}$), 15% naphtha (C_6H_{14}), and 5% light gases (CH_4).[44,46] No carbon loss is considered during the hydrocracking process, which is consistent with experimental results.[48] The H_2 consumption for the wax hydrocracking reaction is assumed to be equal to the stoichiometric amounts required for the aforementioned carbon yields. The estimated H_2 requirement (1.25 wt % of the feed wax) is provided by the unconverted reactant present in the FT exhaust gas.

Separation

In general, the separation and purification of products from a chemical reaction involve a series of elaborate processing steps, each of which requires additional energy input.[18,31] However, for the preliminary process synthesis, we anticipate that the influence of well-established hydrocarbon-gas-water separation schemes will be small on the overall solution. Therefore, we have only modeled a three-phase separator using vapor–liquid–liquid equilibrium that separates the three phases namely gas, aqueous, and organic liquid (consisting of condensable hydrocarbons) phases. Although such a separation does not produce a high purity product, we are able to model a thermodynamically feasible separation which can be achieved in a single stage and does not require additional energy usage.

Each separation unit is operated at a fixed temperature and pressure, which is determined from rigorous Aspen Plus® simulations of model feeds to allow for maximum fuel recovery and by-product recycle. Because of the low solubility of hydrocarbons and other gases in water, the aqueous liquid phase is approximated by water. The resulting phase equilibrium between the aqueous phase and the vapor phase is modeled using Raoults law. For each component j, the equilibrium separation factor corresponding to the vapor-organic liquid phase equilibrium (Eq. 3), K_j^{sep}, is assumed to be constant. For the fixed temperature and pressure of the separation units, the values for K_j^{sep} are derived from rigorous flash calculations of a model feed using the Peng–Robinson equation of state with Boston–Mathias alpha function in Aspen Plus®.[33] The assumption of a constant K_j^{sep} is reasonable because the feed molar compositions feasible to the optimization do not vary greatly from the model feed compositions used. In particular, the variation in the feed mole fraction of the components distributing between the organic liquid and vapor phases is relatively small due to the large amounts of water present in the feed (~40–50 mol %). For separations with large variations in the feed composition, the constant K_j^{sep} assumption will not hold and more detailed models incorporating the effect of composition would be needed

$$\forall(u,udd) \in \text{vapor streams}, \forall(u,ud) \in \text{organic liquid streams},$$
$$x_{u,udd,j} = K_j^{\text{sep}} x_{u,ud,j} \tag{3}$$

Heat and power integration

The rate of external heat supply for an augmented process can be minimized by exchanging heat between the available heat sources and sinks subject to a minimum temperature of approach for heat transfer (Table 4). For fixed process operating variables, the minimum heating and cooling requirements are calculated by identifying the corresponding process pinch temperature. The pinch temperature refers to the temperature value at which the process composite hot and cold enthalpy curves are separated by the minimum temperature of approach $\Delta T_{\min}$.[50] For simultaneous heat and mass integration involving variable process flow rates and compositions, the minimum heating and cooling

Table 4. Main Parameters-Heat Integration and Optimization

Parameter	Symbol	Values
Heat and Power Integration		
Condenser pressure	*pco*	0.03 bar, 0.1 bar
Minimum temperature of approach	$\Delta T_{\min}$	10 K
Boiler pressure	*pb*	80 bar, 160 bar
Turbine inlet temperature	*Th*	700 K, 800 K
Maximum steam flow rate	$n_{\mathrm{fl}}^{\max}$	2 kmol/h
Maximum Rankine cycles	$E_{\mathrm{eng}}^{\max}$	3
Combustion heat recovery	$\eta_{\mathrm{ht,rec}}$	80%
Heat exchanger maximum temperature[49]		1073 K
Objective Function		
Sun-to-H_2 efficiency	$\eta_{\mathrm{H_2}}$	6.2%
Sun-to-heat	η_{heat}	37.5%
Sun-to-electricity	η_{E}	10%
BARON Parameters		
Local solvers		CONOPT, MINOS
Relative optimality tolerance		10^{-4}

All the flow rates are normalized to 1 kmol/h of biomass carbon feed processed. Multiple values (separated by commas) considered for certain parameters.

requirements can be calculated by identifying the pinch temperature using the constraints proposed by Duran and Grossmann.[51] These constraints, when included in an MINLP model, serve to identify the process pinch temperature among a set of candidates, deemed to be the inlet temperature of the hot and cold process streams and sources (see Supporting Information). The minimum gross heating requirement is supplied at the highest temperature of the process, which is the operating temperature of the heat-assisted gasifier (1400 K). This gross heating requirement can be supplied by a combination of the heat recovered from combustion of the purge streams, Q_{comb}, and solar-derived heat Q_{hutil}, as reflected in the constraint of Eq. 4. Here, $Q_{\mathrm{hutil,gross}}$ is the maximum of the minimum gross heating requirement and the heat recovered from purge stream combustion (see Supporting Information). The combustion (using air) of the process purge streams is modeled by allowing a fraction of total energy content of the purge streams (η_{htrec}) to be available at the highest temperature of the process (Eq. 4). Here, η_{htrec} accounts for the energy losses (e.g., sensible heat losses in the air stream) during combustion heat recovery

$$Q_{\mathrm{hutil}} \geq Q_{\mathrm{hutil,gross}} - \eta_{\mathrm{htrec}} Q_{\mathrm{comb}} \tag{4}$$

We also allow for simultaneous power generation from the waste heat using a set of predefined Rankine cycles with different operating boiler pressures (*pb*), condenser pressures (*pco*), and turbine inlet temperatures (*th*) as proposed by Elia et al.[52] Subsequently, the power generated from these cycles can be scaled according to the water flow rate.[52] As a modification from the method of Elia et al., we model the use of condensing turbines with exhaust pressures much below ambient pressure to improve power recovery (Table 4). Rankine cycles with turbines producing low-pressure steam are not considered here, as any low temperature heat demand can be met using available process heat sources (see Figure 2). As the temperatures of the streams of the predefined Rankine cycles are also known, these streams are allowed to exchange heat with other process streams and point sources in the heat integration scheme.[17,52] Binary decision variables ($y_{pb,pco,th}$) determine the presence or absence of the defined Rankine cycles in the process. Equations 5 and 6 define the upper bounds on the number of Rankine cycles allowed and the steam molar flow rate in each cycle ($n_{pb,pco,th}$). The net external electric power to be supplied from solar energy (W_{net}), is defined as the difference of the power consumption via compressors, pumps, and the Rectisol unit (W_{rec}) and the power generated by the steam cycles (Eq. 7)

$$\sum_{(pb,pco,th)} y_{pb,pco,th} \leq E_{\mathrm{eng}}^{\max} \tag{5}$$

$$n_{pb,pco,th} \leq n_{\mathrm{fl}}^{\max} y_{pb,pco,th} \ \forall (pb,pco,th) \tag{6}$$

$$W_{\mathrm{net}} = \sum_{\mathrm{comp}\,(u)} W_u + W_{\mathrm{rec}} - \sum_{(pb,pco,th)} n_{pb,pco,th} w_{pb,pco,th} \tag{7}$$

Objective function

For a target process carbon recovery, η_{carbon}, the objective function to be minimized corresponds to the total solar energy input rate to the process. This includes the solar energy used for supplying H_2, high temperature heat, and electricity, given by the first, second, and third terms on the right-hand side of Eq. 8, respectively. For liquid fuel production, W_{net} is constrained to be nonnegative. Relaxing this constraint will allow for simultaneous liquid fuel and power production as discussed later on. The estimated solar energy conversion efficiencies to H_2 ($\eta_{\mathrm{H_2}}$), heat (η_{heat}), and electricity (η_{E}) used are shown in Table 4 and represent currently feasible solar conversion efficiencies (see Supporting Information)

$$Q_{\mathrm{solar}} = \mathrm{LHV}_{\mathrm{H_2}} m w_{\mathrm{H_2}} \frac{\sum_{\mathrm{str}\,(rh2,udd)} f_{rh2,udd}}{\eta_{\mathrm{H_2}}} + \frac{Q_{\mathrm{hutil}}}{\eta_{\mathrm{heat}}} + \frac{W_{\mathrm{net}}}{\eta_{\mathrm{E}}} \tag{8}$$

Bounding constraints

For the overall process, we impose the target process carbon recovery constraint of Eq. 9. The first and second summations on the left-hand side of Eq. 9 refer to the total carbon recovered in the liquid fuel produced from FT synthesis/hydrocracking and H_2Bioil process, respectively. All the molar flow rates of the process are normalized to 1 kmol/h of biomass carbon feed processed

$$\sum_{\mathrm{fuelft}\,(j)} n_{\mathrm{fl}\,1,pdi,j} \phi_{\mathrm{carbon},j} + \sum_{\mathrm{fuelhyp}\,(j)} n_{\mathrm{fl}\,2,pgas,j} \phi_{\mathrm{carbon},j} = \eta_{\mathrm{carbon}} \tag{9}$$

$$\begin{aligned} &\mathrm{CH}_{1.44}\mathrm{O}_{0.60} + x_1\mathrm{H}_2 + x_2\mathrm{O}_2 \rightarrow x_3\mathrm{CH}_{1.46}\mathrm{O}_{0.01} \\ &+ x_4\mathrm{CH}_{2.13} + x_5\mathrm{CO}_2 + x_6\mathrm{H}_2\mathrm{O} \end{aligned} \tag{10}$$

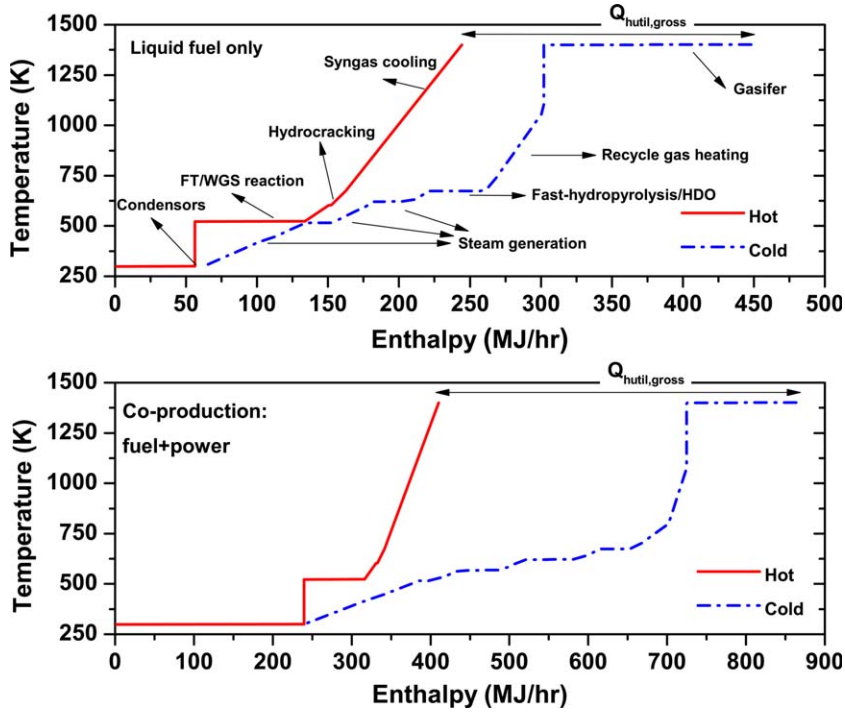

Figure 2. Hot and cold composite curves for the optimal process configuration for $\eta_{carbon} = 80\%$ for liquid fuel production only (top) and liquid fuel and power production (bottom); $\alpha = 0.95$, $\eta_{carbon,hyp} = 48\%$.

[Color figure can be viewed in the online issue, which is available at wileyonlinelibrary.com.]

$$\begin{gathered}\text{Minimize } x_1\\ \text{Subject to}\\ x_3+x_4=\eta_{\text{carbon}}\\ x_3+x_4+x_5=1\\ -2x_1+1.46x_3+2.13x_4+2x_6=1.44\\ -2x_2+0.01x_3+2x_5+x_6=0.60\\ x_3 \le \eta_{\text{carbon ,hyp}}\\ x_1,x_2,x_3,x_4,x_5,x_6 \ge 0\end{gathered} \tag{11}$$

We also include constraints, which provide lower bounds on the process H_2 and solar heat requirements. For a specific value of η_{carbon}, the process H_2 consumption has to be greater than the theoretical minimum H_2 consumption defined from the overall process reaction in Eq. 10. The first term on left-hand side of Eq. 10 refers to biomass. The reactant O_2 is sourced from air and enables the combustion of all the process purge streams for heat recovery. Thus, those carbon and hydrogen atoms not recovered as liquid fuel are lost as CO_2 and H_2O, respectively. On the right side of Eq. 10, the first and second lumped molecular formulas correspond to the liquid fuel produced from the H_2Bioil process (formula from Table 2) and FT synthesis/hydrocracking, respectively. The theoretical minimum H_2 consumption is calculated as the optimal objective function value of the linear program given in Eq. 11, with the constraints including atom balances and the maximum carbon recovery as liquid fuel for the fast-hydropyrolysis/HDO reaction.

We can lower bound the gross process heating requirements with the highest temperature heat sink, which in case of the H_2Bioil-STG superstructure, is the gasifier heat duty. Together, Eqs. 4 and 12 indirectly lower bound the solar heat requirement for the process

$$Q_{\text{hutil,gross}} \ge q_{gfy} \tag{12}$$

Model summary

The developed mathematical model is a nonconvex MINLP with 8 binary variables, 820 continuous variables and 851 equality and 39 inequality constraints. The model contains 394 nonlinear terms, mostly as bilinear expressions used in defining split fractions, mole fractions, and reaction equilibrium. We solved the model in GAMS[53] for different values of η_{carbon} using the branch-and-bound global optimization algorithm implemented in BARON.[54] Global optimization overcomes the challenges of local optimization solvers which include: (1) being limited to inferior local optimal solutions by virtue of the nonconvex nature of the problem and (2) requiring knowledge of good quality initial solutions, which is particularly difficult to identify for large-scale process networks. The global optimization algorithm implemented in BARON iteratively generates an improved lower bound on the objective function by solving a convex relaxation of the original nonconvex problem.

In certain cases, the rate of improvement in the lower bound can be increased by adding specific constraints to the convex relaxation of the nonconvex problem. For example, consider the mass balance constraints for each stream splitter unit u in the MINLP model, given by Eqs. 13 and 14. The summation of the split fraction, $\lambda_{u,udd}$, over the set of all outlet streams from the splitter u must be equal to unity (Eq. 14). In Eq. 13, $n_{u,udd,j}$ and $n_{ud,u,j}$ correspond to the component molar flow rate in the outlet stream from the splitter u (connecting to unit *udd*) and the inlet stream to the splitter u (originating from unit *ud*),

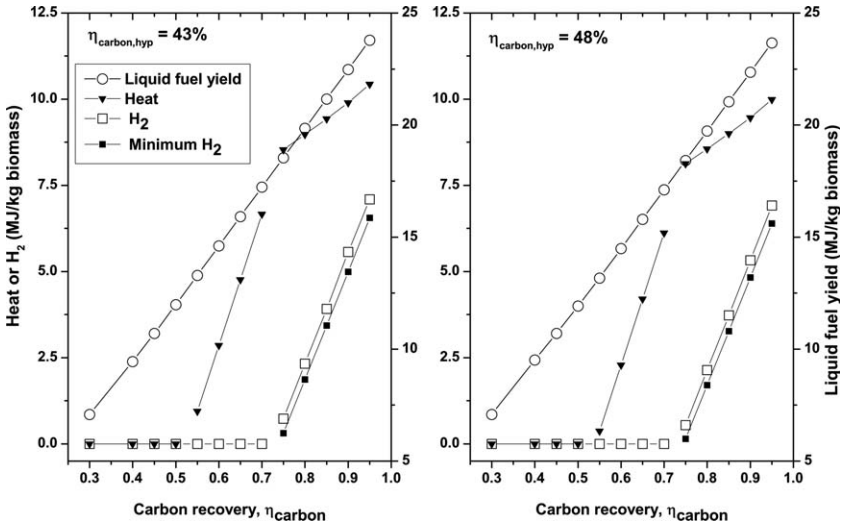

Figure 3. Solar heat, H_2 consumption, and liquid fuel yield of the optimal process configuration for different target carbon recovery levels; $\alpha = 0.95$. Carbon recovery from fast-hydropyrolysis/HDO: $\eta_{carbon,hyp} = 43\%$ (left) and $\eta_{carbon,hyp} = 48\%$ (right).

respectively. Convexification techniques using convex and concave envelopes of the bilinear term in Eq. 13 lead to mass balance violations in the convex relaxation. In contrast, addition of the individual component mass balance constraint (Eq. 15) for the set of all components in the convex relaxation improves the quality of the lower bound by preventing mass balance violation and thereby helps to reduce the computational time required for the solution.[54,55]

$$\forall u \in \text{split}(u), udd \in \text{str}(u, udd), ud \in \text{str}(ud, u), j \in \text{inspec}(u, j)$$

$$n_{u,udd,j} = \lambda_{u,udd} n_{ud,u,j} \tag{13}$$

$$\sum_{\text{str}(u,udd)} \lambda_{u,udd} = 1 \tag{14}$$

$$\sum_{\text{str}(u,udd)} n_{u,udd,j} = n_{ud,u,j} \tag{15}$$

We also include a constraint in the relaxation that limits the energy efficiency of the overall process, defined as the ratio of the lower heating value (LHV) of the product (liquid fuel) to the LHV of biomass and H_2 feeds as well as electricity and heat input, to be less than 100%. Such a constraint provides a nonredundant linear relation between the key process variables in the relaxation of the original nonconvex formulation. This constraint is shown in Eq. 16, where Q_{cutil} refers to the process cooling requirement and the first and second terms of the right-hand side refer to the heating value of the liquid fuel produced from the H_2Bioil process and FT/hydrocracking, respectively. The two summations on the left-hand side of Eq. 16 correspond to the energy input as H_2 and biomass

$$\begin{aligned} Q_{\text{hutil}} + W_{\text{net}} + \text{LHV}_{\text{H}_2} mw_{\text{H}_2} \sum_{\text{str}(rh2,udd)} f_{rh2,udd} \\ + \text{LHV}_{\text{bio}} mw_{\text{bio}} \sum_{\text{str}(rbi,udd)} n_{rbi,udd,bio} \\ \geq \sum_{\text{fuelhyp}(j)} n_{\text{fl}2,pgas,j} \text{LHV}_j mw_j \\ + \sum_{\text{fuelft}(j)} n_{\text{fl}1,pdi,j} \text{LHV}_j mw_j + Q_{\text{cutil}} \end{aligned} \tag{16}$$

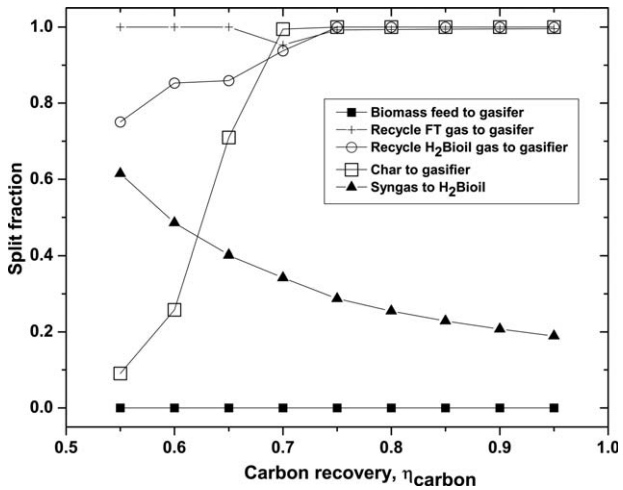

Figure 4. Split fraction of the optimal process configuration for different target carbon recovery levels; $\eta_{carbon,hyp} = 48\%$; increase in carbon recovery beyond 50% is via FT synthesis.

Results and Discussion

General results

Figures 2–4 summarize the heat integration, supplemental energy consumption, and process topology of the optimal process configuration for different values of η_{carbon}. The presented solutions of the MINLP model refer to a process producing liquid fuel exclusively, corresponding to an objective function value which is greater than or equal to zero. In general, the optimal solutions favor feeding biomass to the H_2Bioil process over the heat-assisted gasifier (Figure 4) because of the higher carbon and energy efficiency of the former thermochemical conversion pathway.[27] Consequently, the optimal solution for each value of η_{carbon} is sensitive to the variation in the H_2Bioil carbon recovery as liquid, $\eta_{\text{carbon,hyp}}$, as illustrated in Figure 3. For example, at $\eta_{\text{carbon}} = 55\%$, the optimal solar heat requirement for $\eta_{\text{carbon,hyp}} = 43\%$ is nearly two and half times the

Table 5. Optimal Process Split Fractions and Steam Requirement for Gasification in the Case of $\eta_{carbon} = 50\%$

		Process Split Fractions (%)						
		Syngas to		Feeds to Gasifier				
$\eta_{carbon,hyp}$	Steam (kmol/h)	FT	Purge	H_2Bioil Gas	FT Gas	Biomass	Char	Biomass to Purge
43%	0	42.6	0	66.6	100	0	24.1	0
	0.24	46.0	4.9	36.2	100	0	100	3.6
48%	0.82	16.4	0	61.3	100	0	0	0
	0.05	52.1	0	59.5	100	16.0	100	0

All the flow rates are normalized to 1 kmol/h of biomass carbon feed processed. Each row represents one alternative optimal configuration.

corresponding value for $\eta_{carbon,hyp} = 48\%$. In contrast, the sensitivity of the optimal solution to the variation in FT synthesis chain growth probability (α) is relatively small and, therefore, has not been presented here.

For all cases of η_{carbon} studied here, the optimal process configuration requires zero solar electricity input, as the process electrical power requirement is supplied from utilizing the waste heat through the available Rankine cycles. The developed MINLP model is also capable of identifying processes that coproduce electricity and liquid fuel, in case such a process is deemed economical. When allowing for coproduction, we find that the optimal process configuration has the same process topology and similar flow rates as the optimal configuration that is constrained to not produce any electricity. However, as the Rankine cycles are operated at their maximum working fluid capacity (Eq. 6) to produce excess power, the process with coproduction consumes additional solar heat compared to the liquid fuel solution. This fact is illustrated in Figure 2 where the heat integrations of the optimal process configurations for the liquid fuel only and coproduction case are depicted. As seen in Figure 2, the additional solar heat that is soaked up for the coproduction of power is used to generate superheated steam (700–800 K) for the Rankine cycles. This finding suggests that the electrical power produced from soaking additional solar heat via the Rankine cycle has a higher sun-to-electricity efficiency than the specified external solar electricity available at $\eta_E = 10\%$. In case of the optimal process configuration producing liquid fuel alone, Figure 2 also suggests that the gross heat input (purge combustion heat and solar heat) is primarily used to heat the feed streams to the gasifier beyond 673 K and to supply the heat duty for gasification and fast-hydropyrolysis/HDO. In one possible design, the external heat can be supplied indirectly via circulating bed material to a consolidated reactor unit involving a top fast-hydropyrolysis zone operating at 673 K and a bottom gasification zone operating at 1400 K. The cold feed streams can be injected at the appropriate temperature regimes within the reactor.[27]

Standalone process regime

The quantity of solar heat and H_2 input required by the optimal process configuration is dependent, among other factors, on the parameters η_{carbon} and $\eta_{carbon,hyp}$. As seen in Figure 3, the optimal process configurations when $\eta_{carbon} < 55\%$ are standalone processes that do not require any solar energy input, either as heat or H_2. This would correspond to $Q_{hutil} = 0$, and $Q_{hutil,gross} = \eta_{htrec} Q_{comb}$ in Eq. 4. At the maximum value of η_{carbon} for a standalone process, given by $\eta_{carbon} = 54\%$ ($\eta_{carbon,hyp} = 48\%$), the heat available from the combustion of the residual carbon and hydrogen containing purge streams (char and gas by-products) is equal to the minimum process heat requirements. At lower values of η_{carbon}, the optimal standalone process produces excess heat at the expense of reducing the liquid fuel output.

It is interesting to note that when $\eta_{carbon} \leq 54\%$, the MINLP model finds multiple optimal process configurations that have different process topologies and steam requirement for gasification, but have the same objective function value (= 0). For $\eta_{carbon} = 50\%$, Table 5 describes some alternative process configurations, in terms of their key split fractions and gasification steam requirements. For each value of $\eta_{carbon,hyp}$, different combinations of char and gas (syngas or recycle gas) can be combusted to provide the process heat requirements. Similarly, the H_2 requirement for the H_2Bioil process is met by the H_2 and CO in the syngas produced from gasifying one or more of the following: a portion of the biomass, recycled char, and/or gas. The role of steam feed to the gasifier is primarily to convert the char, biomass, and recycled hydrocarbons to H_2 and CO in the syngas mixture. Eventually, the most preferred among all the optimal process configurations will be the one with the least capital and operating cost. For example, doing away with the capital intensive syngas-to-liquid fuel equipment (e.g., acid gas cleaning, FT synthesis, etc.) yields a standalone process with $\eta_{carbon} \sim 48\%$ ($\eta_{carbon,hyp} = 48\%$). Here, the entire biomass is fed to the H_2Bioil process, and the H_2 requirement is supplied from the syngas produced from gasifying 100% of the char and 19% of the recycle gas streams.

Augmented process regime

As can be seen in Figure 3, for the $\eta_{carbon} \geq 55\%$ cases studied here, the optimal process configurations require additional energy input because a reduced amount of carbon is available for providing process heat via combustion. Here, solar heat, which is available at a higher solar conversion efficiency than H_2 or electricity, supplies the remaining portion of the process heat. The solar heat input is predominantly used to supply the heat duty needed for gasification which, in the case of $55\% \leq \eta_{carbon} \leq 70\%$, is required for the reforming reactions of the recycled char and gas streams. The syngas produced from the gasifier is subsequently split between the H_2Bioil process for H_2 supply and FT synthesis/hydrocracking for liquid fuel production. From Figures 3 and 4, the following are the major topological trends for the optimal process configurations with increasing values of η_{carbon} (in the range of 55–70%). (1) A higher fraction of char and gas by-products need to be recycled to the gasifier (Figure 4), resulting in correspondingly higher solar heat requirements (Figure 3). For additional carbon recovery, the recycling of gas streams produced from the H_2Bioil process and FT synthesis (composed mainly of CO_2 and C_1–C_4

hydrocarbons) is favored over recycling of char. The recycled C_1—C_4 hydrocarbons and CO_2 can be reformed to H_2 and CO without the need to supply external steam to the gasifier. In contrast, to use char, external steam has to be supplied to convert it to H_2 and CO. The generation of this steam requires additional heat and this penalizes the use of char. (2) Higher fractions of syngas are used for liquid fuel production via FT synthesis, resulting in an increasing fraction of biomass carbon being recovered as FT liquid fuel. Despite this, the optimal process configuration remains self-sufficient in H_2 until η_{carbon} increases close to 70%. This is achieved by recycling 100% of the char as well as H_2Bioil and FT gas by-products to be reformed in the gasifier.

When $\eta_{carbon} > 70\%$, the carbon that is not converted to fuel exists predominantly as CO_2 which accumulates as an inert in the process streams and cannot be recovered by recycling alone. In the absence of external H_2, CO_2 formation acts as a sink for rejecting the large amount of oxygen present in the feed biomass. Consequently, for $\eta_{carbon} > 70\%$, the process requires both solar heat and H_2 input to get rid of the biomass oxygen as H_2O rather than as CO_2. The solar H_2 is supplied to the gasifier rather than the H_2Bioil process to allow for the conversion of the residual CO_2 (built up in the recycled gas streams) to CO via the Reverse Water-Gas Shift (RWGS) reaction. The enthalpy change of the RWGS reaction is relatively small compared to the reforming reaction ($\sim$30 kJ/mol vs. $\sim$300 kJ/mol), which was dominant during gasification in the regime of $\eta_{carbon} \leq 70\%$. This change in gasification reaction chemistry when η_{carbon} increases beyond 70% explains the reduction in the slope of the solar heat requirement curve in Figure 3. The additional CO produced from the RWGS reaction provides an indirect source of H_2 for the H_2Bioil process (via WGS reaction) and also reacts with H_2 to produce liquid fuel during FT synthesis. In this manner, the process solar H_2 requirement can be minimized to be close to the theoretical minimum value for every $\eta_{carbon} > 70\%$ as shown in Figure 3. For $70\% \leq \eta_{carbon} \leq 95\%$ cases, the unconverted carbon is purged from the process in the form of pure CO_2 separated from the syngas in the acid gas removal unit (during syngas cleaning).

Comparison with gasification-FT

We compare the optimal processes obtained from evaluating the H_2Bioil-STG superstructure against the optimal STG-FT processes. This comparison quantifies the potential benefit of integrating different biomass thermochemical pathways for liquid fuel production.

The STG-FT optimal process configuration is derived by restricting the feasible region of the developed MINLP model to the heat-assisted gasification/FT part of the H_2Bioil-STG superstructure (Figure 1). For each value of η_{carbon}, the key variables in the optimization include: (1) the distribution of the feed biomass between gasification and combustion (via purge) for process heat, (2) the extent of FT by-product gas recycling and residual CO_2 recycling, (3) the steam requirement for the gasifier and the WGS reactors, and (4) the process heat and H_2 input. Of particular note is the case of $\eta_{carbon} = 30\%$, where the MINLP model finds alternative optimal configurations which do not require any solar energy input. For one configuration shown in Figure 5, 22% of the feed biomass is combusted for process heat and 53% of the vapor stream from the vapor–liquid separation unit is recycled to the gasifier to generate additional syngas. With increasing

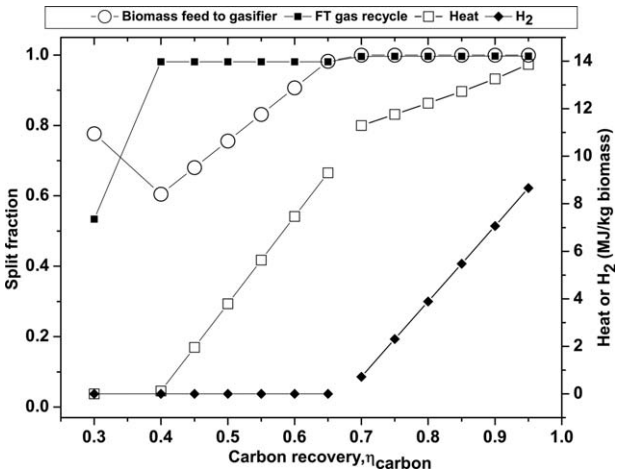

Figure 5. Key split fractions (left *Y* axis) and solar heat and H_2 consumption (right *Y* axis) of the optimal STG-FT process configuration for different target carbon recovery levels, $\alpha = 0.95$.

$\eta_{carbon} \geq 40\%$, an increased fraction of biomass is used for gasification, along with recycling of the unconverted reactants and by-products of FT synthesis as seen in Figure 5. The variation in solar heat and H_2 consumption versus carbon recovery follow similar trends to that seen for the H_2Bioil-STG superstructure. A detailed discussion of the main characteristics of the biomass gasification-FT process is available elsewhere and is, therefore, omitted.[13,17,24,31]

Every feasible solution to the STG-FT process optimization provides a suboptimal solution to the H_2Bioil-STG superstructure optimization. In fact, the amount of heat and H_2 required for the optimal STG-FT processes are found to be consistently higher than the requirements estimated for the optimal H_2Bioil-STG processes (Figure 5 vs. Figure 3). Although the optimal H_2Bioil-STG process remains standalone for cases of $\eta_{carbon} \leq 54\%$ in Figure 3, the STG-FT process requires solar heat input for $\eta_{carbon} \geq 40\%$. As shown in Figure 6, for $70\% \leq \eta_{carbon} \leq 95\%$, the optimal solution of the H_2Bioil-STG process results in $\sim$28–156% lower solar energy requirement relative to the STG-FT process. As expected and also depicted in Figure 6, solar energy input to the STG-FT process increases with a decrease in FT α, because increasing amounts of C_1—C_{10} hydrocarbons have to be recycled to the gasifier.

Accounting for intermittent solar energy

For enabling augmented biofuel production using intermittent solar energy, any combination of the following storage options could be used: (1) during the periods when solar energy is available (day time), it is stored in a suitable form to supply heat and H_2 at other times or (2) during the periods when solar energy is unavailable (night time), the unconverted carbon (e.g., char or gas) is stored for subsequent conversion to liquid fuel. Recently, a high efficiency energy and carbon storage concept based on the cyclic transformation between carbon dioxide and carbonaceous molecules like methane was proposed for uninterrupted renewable power generation.[16] This storage concept can be adapted for round the clock augmented biofuel production, as shown in Figure 7. During the day time, biomass and stored liquid CO_2 (produced in the night time) can be converted to liquid fuel and a carbonaceous molecule using solar heat and/

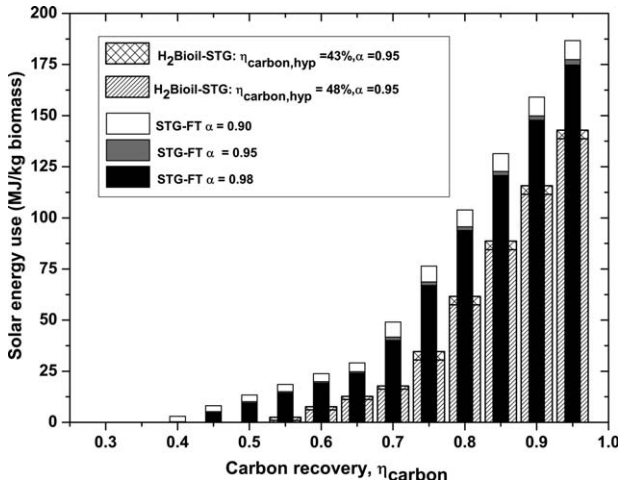

Figure 6. Solar energy consumption of the optimal H_2Bioil-STG and STG-FT process configurations for different target carbon recovery levels; Solar energy conversion efficiencies reported in Table 4.

or H_2. The produced carbonaceous molecule is liquefied and stored for use in the night time, where it provides the necessary supplemental energy to augment biomass conversion to liquid fuel. The unconverted carbon from the process in the night time is captured as CO_2, which is liquefied and stored for use in the day time. In this manner, the biofuel facility can be operated to achieve higher than standalone η_{carbon}. Modeling results for the process of Figure 7 will be presented in a subsequent publication. A key aspect of the process is the choice of carbonaceous molecule and its impact on the supplemental solar energy consumption.[16]

Conversely, if cost-effective energy or carbon storage options are not available, the flexibility to operate a biofuel facility at different carbon recovery levels can allow for continuous operation without start-up/shutdown issues. Using the results in Figures 3–6, we can construct flexible biofuel process designs that are capable of operating in augmented (high η_{carbon}) or standalone (low η_{carbon}) mode depending on whether or not supplemental solar heat and H_2 are available. For the standalone mode of the process, the char and recycle gas will be used to supply the H_2 required for the H_2Bioil process (via syngas generation) and process heat (via combustion), resulting in a maximum standalone η_{carbon} of ~52–54% (for $\eta_{carbon,hyp}$ =43–48%). In the augmented mode of the process, use of solar heat allows the recovery of a portion of the carbon in the char and gas streams as liquid fuel using FT synthesis, thereby resulting in η_{carbon} of ~73–74% ($\eta_{carbon,hyp}$ = 43–48%). When use of both solar heat and H_2 is economical, the process may further be augmented to operate at $\eta_{carbon} > 74\%$. In this augmented mode, the process economics will determine the η_{carbon} that is chosen. It should be noted that in case FT synthesis is found to be uneconomical for a small-scale biofuel facility, then the H_2Bioil process and the heat-assisted gasifier can be operated round the clock in a standalone mode, at a carbon recovery, that is primarily dependent on the parameter, $\eta_{carbon,hyp}$. The optimization of HDO catalysts and fast-hydropyrolysis operating conditions could potentially increase $\eta_{carbon,hyp}$. However, beyond a certain $\eta_{carbon,hyp}$, the by-product char and gas will be insufficient to supply the necessary heat and H_2, and supplemental energy input would be necessary.

Conclusions

We have computationally demonstrated a method to systematically identify carbon and energy efficient biofuel processes using supplemental solar energy available as heat or H_2. The method relies on the heuristic design of a novel process superstructure, which considers one or more biomass conversion pathways and their possible integrations.

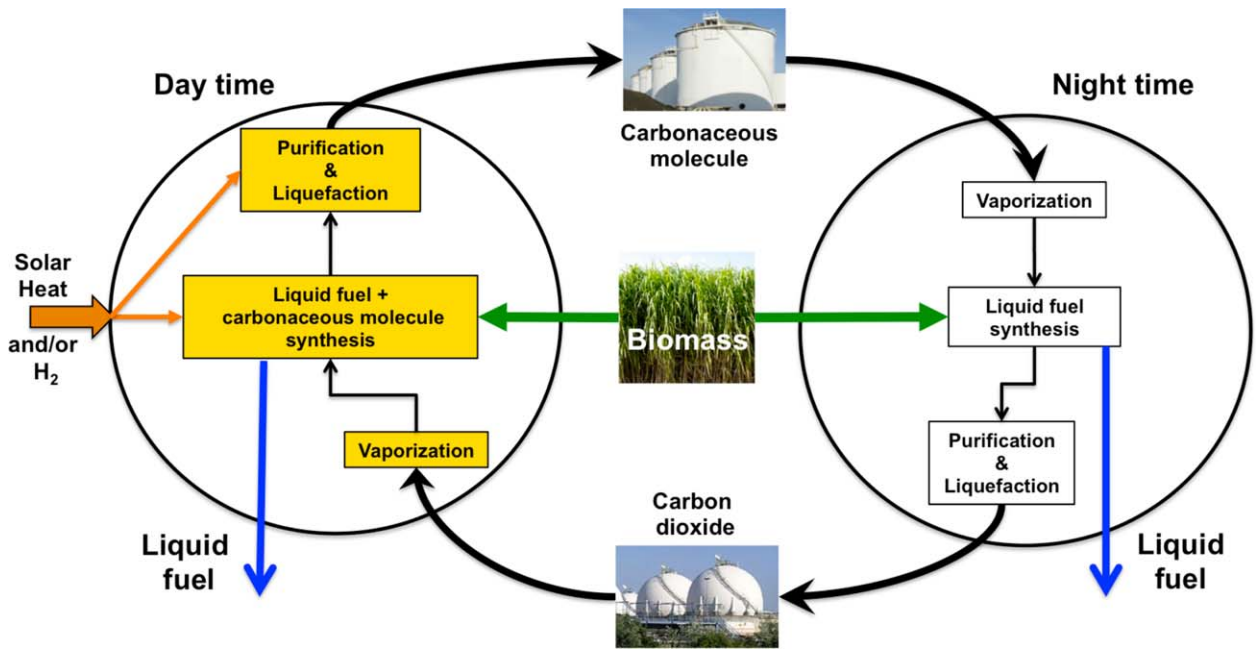

Figure 7. Process for round the clock operation of an augmented biofuel process using combined energy and carbon storage.

[Color figure can be viewed in the online issue, which is available at wileyonlinelibrary.com.]

Subsequently, the developed process superstructure is represented as a nonconvex MINLP model that allows for simultaneous heat, mass, and power integration. This MINLP is then solved using global optimization tools to identify promising process configurations for different target carbon recovery cases.

Synergistic process integrations are possible from simultaneously evaluating different biomass thermochemical conversion pathways like fast-hydropyrolysis/HDO and gasification-FT. From a topological standpoint, the optimal process configurations favor: (1) feeding biomass to the H_2Bioil process as against the heat-assisted gasifier and (2) using char and gas by-products for producing heat, H_2, or additional liquid fuel via FT synthesis. Depending on the target carbon recovery constraint, the optimal process configuration is either a standalone process ($\eta_{\text{carbon}} \leq 54\%$), an augmented processes that uses solar heat ($54\% \leq \eta_{\text{carbon}} \leq 74\%$) or an augmented process that uses both solar heat and H_2 ($74\% \leq \eta_{\text{carbon}} \leq 95\%$). For the last class of processes, the H_2 consumption is verified to be close to the theoretical minimum H_2 consumption.

We also suggest flexible biofuel processes capable of operating at low and high carbon recovery levels to account for the intermittent availability of supplemental solar heat or H_2. Based on the H_2Bioil-STG superstructure, a biofuel facility without energy or carbon storage capabilities can operate at values of η_{carbon} close to 52–54% in the absence and at higher carbon recovery levels in the presence of supplemental solar energy (heat and/or H_2). The long-term viability of such flexible biofuel processes will depend on overcoming the engineering challenges encountered in building such facilities as well as the economic tradeoff when compared to the processes operating round the clock using energy/carbon storage facilities.

Acknowledgments

Discussions with Professors W. Nicholas Delgass and Fabio H. Ribeiro are gratefully acknowledged. Research supported as part of the Center for Direct Catalytic Conversion of Biomass to Biofuels, an Energy Frontier Research Center funded by the U.S. Department of Energy (DOE), Office of Science, Basic Energy Sciences (BES), under Award # DE-SC0000997; by the U.S. DOE under Award # DE-FG-3608GO18087; by the National Science Foundation EFRI (0938033-DGE) and Solar Economy IGERT (0903670-DGE). This contribution was identified by Thomas A. Adams II (McMaster University) as the Best Presentation in the session "Process Design I" of the 2012 AIChE Annual Meeting in Pittsburgh, PA.

Notation

$\beta_{i,k}$ = moles of atom k (= C,H, or O) in one mole of component i; negative for reactants and positive for products in Eq. 1
$\lambda_{u,udd}$ = split fraction of the stream connecting splitter u with the downstream unit *udd*
$\phi_{\text{carbon},j}$ = moles of carbon present in one mole of component j
b_i = for i = 2, 4, …, 9, molecular weight ratio of component i to biomass (moisture and ash free); b_3 = 1 (see Supporting Information)
comp(u) = set of all pump and compressor units
$f_{u,udd}$ = stream molar flow rate between unit u and unit *udd*
fl1, fl2 = separation units
fuelft(j) = set of all components in FT diesel
fuelhyp(j) = set of all components in H_2Bioil liquid fuel
gfy = heat-assisted gasifier unit
inspec(u,j) = components present in the input stream to unit u
K_j^{sep} = equilibrium separation factor for component j
LHV_j = lower heating value of component j in MJ/kg. j = H_2, bio…
m_{exp} = number of experimental datasets
mw_j = molecular weight of component j in kg/kmol. j = H_2, bio…
$n_{pb,pco,th}$ = molar flow rate of steam in Rankine cycle (*pb*, *pco*, *th*)
$n_{u,udd,j}$ = component j molar flow rate between unit u and *udd*
pdi = FT diesel storage tank
*p*gas = H_2Bioil liquid fuel storage tank
Q_{comb} = heat available from purge stream combustion
Q_{cutil} = process cooling requirement
$Q_{\text{hutil,gross}}$ = maximum of the minimum gross heating requirement and the heat recovered from purge stream combustion
Q_{hutil} = minimum solar heat requirement
q_u = heat duty of unit u
rbi = biomass feed hopper
*rh*2 = solar H_2 generation source
split(u) = set of all splitter units
str(u,*udd*) = set of streams connecting unit u and *udd*
u,*ud*, or *udd* = units of the process
W_u = electrical power input to pump/compressor u
$w_{3,j}^{\text{exp}}$ = carbon recovery as liquid for experimental dataset j
$w_{\text{i,j}}^{\text{exp}}$ = for i = 2, 4, …, 9 weight ratio of component i to biomass (moisture and ash free basis) for dataset j (see Supporting Information Table S6)
W_{net} = net process power input
$w_{pb,pco,th}$ = parameter corresponding to specific power output of Rankine cycle (*pb*, *pco*, *th*)
W_{rec} = electrical power input to Rectisol unit
$x_{u,udd,j}$ = mole fraction of component j in stream connecting separator u with unit *udd*
$y_{pb,pco,th}$ = binary variable for presence or absence of Rankine cycle
z_i = stoichiometric coefficients in Eq. 1.

Literature Cited

1. Cook TR, Dogutan DK, Reece SY, Surendranath Y, Teets TS, Nocera DG. Solar energy supply and storage for the legacy and nonlegacy worlds. *Chem Rev*. 2010;110(11):6474–6502.
2. Lewis NS, Nocera DG. Powering the planet: chemical challenges in solar energy utilization. *Proc Natl Acad Sci USA*. 2006;103(43):15729–15735.
3. Agrawal R, Singh NR. Solar energy to biofuels. *Annu Rev Chem Biomol Eng*. 2010;1(1):343–364.
4. Searchinger T, Heimlich R, Houghton RA, Dong F, Elobeid A, Fabiosa J, Tokgoz S, Hayes D, Yu TH. Use of U.S. croplands for biofuels increases greenhouse gases through emissions from land-use change. *Science*. 2008;319(5867):1238–1240.
5. Tilman D, Hill J, Lehman C. Carbon-negative biofuels from low-input high-diversity grassland biomass. *Science*. 2006;314(5805):1598–1600.
6. NRC. *Liquid Transportation Fuels from Coal and Biomass: Technological Status, Costs, and Environmental Impacts*. Washington, DC: National Academies Press, 2009.
7. Larson ED. A review of life-cycle analysis studies on liquid biofuel systems for the transport sector. *Energy Sustain Dev*. 2006;10(2):109–126.
8. Schubert C. Can biofuels finally take center stage? *Nat Biotechnol*. 2006;24(7):777–784.
9. Downing M, Eaton LM, Graham RL, Langholtz MH, Perlack RD, Turhollow AF Jr, Stokes B, Brandt CC. US billion-ton update: biomass supply for a bioenergy and bioproducts industry. *Technical Report. Oak Ridge National Laboratory (ORNL)*, Oak Ridge, TN, 2011.
10. Mallapragada DS, Singh NR, Agrawal R. Energy systems analysis for a renewable transportation sector. In: Pistikopoulos EN, Georgiadis MC, Kokossis A, editors. *21st European Symposium on Computer Aided Process Engineering-ESCAPE 21*. Chalkidiki, Greece: Elsevier B.V., 2011.
11. Singh NR, Mallapragada DS, Agrawal R, Tyner WE. Economic analysis of novel synergistic biofuel (H_2Bioil) processes. *Biomass Convers Biorefinery*. 2012;2(2):141–148.

12. Brown TR, Brown RC. A review of cellulosic biofuel commercial-scale projects in the United States. *Biofuel Bioprod Biorefin*. 2013; 7(3):235–245.
13. Agrawal R, Singh NR, Ribeiro FH, Delgass WN. Sustainable fuel for the transportation sector. *Proc Natl Acad Sci USA*. 2007;104(12): 4828–4833.
14. Agrawal R, Singh NR. Synergistic routes to liquid fuel for a petroleum deprived future. *AIChE J*. 2009;55(7):1898–1905.
15. Siegel NP, Miller JE, Ermanoski I, Diver RB, Stechel EB. Factors affecting the efficiency of solar driven metal oxide thermochemical cycles. *Ind Eng Chem Res*. 2013;52(9):3276–3286.
16. Al-musleh EI, Mallapragada DS, Agrawal R. Continuous power supply from a baseload renewable power plant. *Appl Energy*. 2014;122: 83–93.
17. Baliban RC, Elia JA, Floudas CA. Optimization framework for the simultaneous process synthesis, heat and power integration of a thermochemical hybrid biomass, coal, and natural gas facility. *Comput Chem Eng*. 2011;35(9):1647–1690.
18. Baliban RC, Elia JA, Floudas CA. Toward novel hybrid biomass, coal, and natural gas processes for satisfying current transportation fuel demands, 1: Process alternatives, gasification modeling, process simulation, and economic analysis. *Ind Eng Chem Res*. 2010;49(16): 7343–7370.
19. Chakravarti S, Bonaquist DP, Drnevich RF, Shah MM. Natural gas enhanced biomass to liquids: project development and modeling. *Comput Chem Eng*. 2012;47:67–75.
20. Baliban RC, Elia JA, Misener R, Floudas CA. Global optimization of a MINLP process synthesis model for thermochemical based conversion of hybrid coal, biomass, and natural gas to liquid fuels. *Comput Chem Eng*. 2012;42:64–86.
21. Baliban RC, Elia JA, Floudas CA. Biomass and natural gas to liquid transportation fuels: process synthesis, global optimization, and topology analysis. *Ind Eng Chem Res*. 2013;52(9):3381–3406.
22. Perkins C, Weimer AW. Solar-thermal production of renewable hydrogen. *AIChE J*. 2009;55(2):286–293.
23. Weimer AW. Solarthermal chemical processing challenges and commercial path forward. *Curr Opin Chem Eng*. 2012;1(3):217–211.
24. Hertwich EG, Zhang X. Concentrating-solar biomass gasification process for a 3rd generation biofuel. *Environ Sci Technol*. 2009; 43(11):4207–4212.
25. Marker TL, Felix LG, Linck MB, Roberts MJ. Integrated hydropyrolysis and hydroconversion (IH2) for the direct production of gasoline and diesel fuels or blending components from biomass, part 1: proof of principle testing. *Environ Prog Sustain Energy*. 2012;31(2): 191–199.
26. Huber GW, Iborra S, Corma A. Synthesis of transportation fuels from biomass: chemistry, catalysts, and engineering. *Chem Rev*. 2006;106(9):4044–4098.
27. Singh NR, Delgass WN, Ribeiro FH, Agrawal R. Estimation of liquid fuel yields from biomass. *Environ Sci Technol*. 2010;44(13): 5298–5305.
28. Roberts M, Marker T, Timber J, Gephart J, Marble B, Stevens J. Biomass to gasoline and diesel using integrated hydropyrolysis and hydroconversion. *Technical Report*. *Des Plaines, IL: Gas Technology Institute*, 2012.
29. Agrawal R, Agrawal M, Singh NR. Process for producing liquid hydrocarbon by pyrolysis of biomass in presence of hydrogen from a carbon-free energy source. *US 8*,217,211 B2. 2012.
30. Agrawal R, Singh NR. Integrated gasification—pyrolysis process. *US 8*,217,210 B2. 2012.
31. Kreutz TG, Larson ED, Liu G, Williams RH. Fischer-Tropsch fuels from coal and biomass. *25th Annual International Pittsburgh Coal Conference*. Pittsburgh, PA, 2008.
32. Jones SB, Valkenburg C, Walton CW, Elliott DC, Holladay JE, Stevens DJ, Kinchin C, Czernik S. Production of gasoline and diesel from biomass via fast pyrolysis, hydrotreating and hydrocracking: a design case. Technical Report. *Richland, WA: Pacific Northwest National Laboratory*, 2009. Available at http://www.osti.gov/bridge/servlets/purl/949907-IeELhA/. Accessed on April 3, 2014.
33. Aspen Technology Inc. ASPEN Plus users guide. *Technical Report*. Burlington, MA: Aspen Technology Inc., 2006. Available at http://aspentech.com. Accessed on April 3, 2014.
34. Linstrom PJ, Mallard WG. *NIST Chemistry WebBook*. 2011. Available at http://webbook.nist.gov/chemistry/. Accessed on April 3, 2014.
35. Manganaro J, Chen B, Adeosun J, Lakhapatri S, Favetta D, Lawal A, Farrauto R, Dorazio L, Rosse DJ. Conversion of residual biomass into liquid transportation fuel: an energy analysis. *Energy Fuels*. 2011;25(6):2711–2720.
36. Daugaard DE, Brown RC. Enthalpy for pyrolysis for several types of biomass. *Energy Fuels*. 2003;17(4):934–939.
37. Haryanto A, Fernando SD, Pordesimo LO, Adhikari S. Upgrading of syngas derived from biomass gasification: a thermodynamic analysis. *Biomass Bioenergy*. 2009;33(5):882–889.
38. Prins MJ, Ptasinski KJ, Janssen FJJG. From coal to biomass gasification: comparison of thermodynamic efficiency. *Energy*. 2007;32(7): 1248–1259.
39. Tay DH, Kheireddine H, Ng DK, El-Halwagi MM, Tan RR. Conceptual synthesis of gasification-based biorefineries using thermodynamic equilibrium optimization models. *Ind Eng Chem Res*. 2011; 50(18):10681–10695.
40. Schuster G, Löffler G, Weigl K, Hofbauer H. Biomass steam gasification–an extensive parametric modeling study. *Bioresour Technol*. 2001;77(1):71–79.
41. Lichty P, Perkins C, Woodruff B, Bingham C, Weimer A. Rapid high temperature solar thermal biomass gasification in a prototype cavity reactor. *J Sol Energy Eng*. 2010;132(1):11012–11017.
42. Dietenberger MA, Anderson M. Vision of the U.S. *biofuel future: a case for hydrogen-enriched biomass gasification*. *Ind Eng Chem Res*. 2007;46(26):8863–8874.
43. Eilers J, Posthuma SA, Sie ST. The shell middle distillate synthesis process (SMDS). *Catal Lett*. 1990;7(1):253–269.
44. Steynberg AP, Nel WU, Desmet MA. Large scale production of high value hydrocarbons using Fischer-Tropsch technology. In: Xinhe B, Yide X, editors. *Studies in Surface Science and Catalysis*, Vol. 147. Amsterdam, The Netherlands: Elsevier, 2004:37–42.
45. Espinoza RL, Steynberg AP, Jager B, Vosloo AC. Low temperature Fischer-Tropsch synthesis from a Sasol perspective. *Appl Catal A*. 1999;186(1–2):13–26.
46. Dry ME. The Fischer-Tropsch process: 1950–2000. *Catal Today*. 2002;71(3–4):227–241.
47. Hoek A, Kersten LBJM. The shell middle distillate synthesis process: technology, products and perspective. In: Xinhe B, Yide X, editors. *Studies in Surface Science and Catalysis*, Vol. 147. Amsterdam, The Netherlands: Elsevier, 2004:25–30.
48. Tijmensen MJA, Faaij APC, Hamelinck CN, van Hardeveld MRM. Exploration of the possibilities for production of Fischer Tropsch liquids and power via biomass gasification. *Biomass Bioenergy*. 2002;23:129–152.
49. Heatric Inc. Features and capabilities of high pressure printed circuit heat exchangers (PCHE). Heatric Inc., Poole, United Kingdom, 2013. Available at http://www.heatric.com/index.html. Accessed on April 3, 2014.
50. Gassner M, Maréchal F. Methodology for the optimal thermo-economic, multi-objective design of thermochemical fuel production from biomass. *Comput Chem Eng*. 2009;33(3):769–781.
51. Duran MA, Grossmann IE. Simultaneous optimization and heat integration of chemical processes. *AIChE J*. 1986;32(1):123–138.
52. Elia JA, Baliban RC, Floudas CA. Toward novel hybrid biomass, coal, and natural gas processes for satisfying current transportation fuel demands, 2: Simultaneous heat and power integration. *Ind Eng Chem Res*. 2010;49(16):7371–7388.
53. McCarl B, Meeraus A, van der Eijk P, Bussieck M, Dirkse S, Steacy P, Nelissen F. McCarl GAMS User Guide. *GAMS Development Corporation*, Washington, DC, 2012.
54. Tawarmalani M, Sahinidis NV. *Convexification and Global Optimization in Continuous and Mixed-Integer Nonlinear Programming: Theory, Algorithms, Software, and Applications*. Dordrecht, The Netherlands: Springer, 2002.
55. Quesada I, Grossmann IE. Global optimization of bilinear process networks with multicomponent flows. *Comput Chem Eng*. 1995; 19(12):1219–1242.

Manuscript received Nov. 15, 2013, and revision received Mar. 4, 2014.